Barotropic tide and baroclinic waves observations in the Río de la Plata Estuary

C. G. Simionato,[1,2] V. Meccia,[1] W. Dragani,[3,4,5] and M. Nuñez[1,2]

Received 9 December 2004; revised 10 February 2005; accepted 18 March 2005; published 22 June 2005.

[1] The first long-period ADCP series collected in two locations of the salinity front of the Río de la Plata estuary are explored for periods less than 30 hours. Barotropic velocity shows tidal and mean currents consistent with what is known about the estuarine circulation in tidal and seasonal scales. Baroclinic currents provide the first evidence of the occurrence of internal waves, which can account for half of the total variance. In the northernmost location, predominantly zonal oscillations with semidiurnal period, and oscillations with a dominant meridional component and diurnal period, are found. Whereas the first ones can be related to the semidiurnal tide, the second ones seem to be atmospherically forced by the land/sea breeze. In the southernmost location, more rotational oscillations are observed, with periods around the inertial and diurnal ones. Inertial oscillations could result from wind relaxation, whereas diurnal oscillations also seem to be forced by breeze. Wave activity in the diurnal band was less frequent in the northernmost than in the southernmost location. This can be attributed to less frequent favorable stratification conditions in that area during the observed period. Wave activity in the southernmost location resulted weaker during the observed fall than during the summer. This could be a typical feature given that in autumn both the number of storms destroying the thermohaline structure increases and land/sea breeze is less frequent. This suggests a likely seasonal cycle in the diurnal wave activity in this area, given that those unfavorable conditions are even more marked during winter.

Citation: Simionato, C. G., V. Meccia, W. Dragani, and M. Nuñez (2005), Barotropic tide and baroclinic waves observations in the Río de la Plata Estuary, *J. Geophys. Res.*, *110*, C06008, doi:10.1029/2004JC002842.

1. Introduction

[2] The Río de la Plata (Figure 1) is a shallow and extensive estuary located in the eastern coast of southern South America at approximately 35°S. It has a northwest to southeast oriented funnel shape approximately 300 km long that narrows from 220 km at its mouth to 40 km at its upper end [*Balay*, 1961]. The estuarine area is 35,000 km^2 and the fluvial drainage area is 3.1×10^6 km^2. The system drains the waters of the Paraná and Uruguay rivers, which constitute the second largest basin of South America. As a result, it has a huge discharge with a mean of around 24,000 m^3 s^{-1}, and maximum values as high as 50,000 m^3 s^{-1} under extreme conditions [*Jaime et al.*, 2002].

[3] The estuary is a microtidal system. Tidal waves associated with the South Atlantic amphidromes reach the Continental Shelf break while propagating northward [*Glorioso and Flather*, 1995, 1997; *Simionato et al.*, 2004a]. As they propagate over the Continental Shelf, geographic setting modifies their propagation so that they enter the estuary mainly from the southeast [*Simionato et al.*, 2004a]. The shallow water shortens the wavelength after they enter the estuary; owing to this effect and the considerable length of the estuary, semidiurnal constituents have the unusual feature of a nearly complete a wavelength within the estuary at all times [*Comisión Administradora del Río de la Plata* (*CARP*), 1989; *Simionato et al.*, 2004a]. Tidal amplitudes are generally not amplified toward the upper part. The estuary is long and converges only at its innermost part, where it is extremely shallow and bottom friction plays a fundamental role in controlling the wave amplitude [*Framiñan et al.*, 1999; *Simionato et al.*, 2004a]. The tidal regime in the estuary is mixed, dominantly semidiurnal, with M_2 being the most significant constituent (M_2 has an amplitude of 0.27 m at Buenos Aires); however, there are significant diurnal inequalities, mostly caused by O_1, with an amplitude of 0.15 m [*D'Onofrio et al.*, 1999]. Given that water level is easier to measure than currents, observations of this last variable are scarcer, and much of

[1]Centro de Investigaciones del Mar y la Atmósfera (CIMA/CONICET-UBA), Universidad de Buenos Aires, Buenos Aires, Argentina.
[2]Also at Departamento de Ciencias de la Atmósfera y los Océanos, Facultad de Ciencias Exactas y Naturales (FCEN), Universidad de Buenos Aires, Buenos Aires, Argentina.
[3]Departamento de Ciencias de la Atmósfera y los Océanos, Facultad de Ciencias Exactas y Naturales (FCEN), Universidad de Buenos Aires, Buenos Aires, Argentina.
[4]Also at Servicio de Hidrografía Naval (SHN) and Escuela del Ciencias del Mar (ESCM-INUN) de la Armada Argentina, Buenos Aires, Argentina.
[5]Also at Consejo Nacional de Investigaciones Científicas y Técnicas (CONICET), Buenos Aires, Argentina.

0148-0227/05/2004JC002842

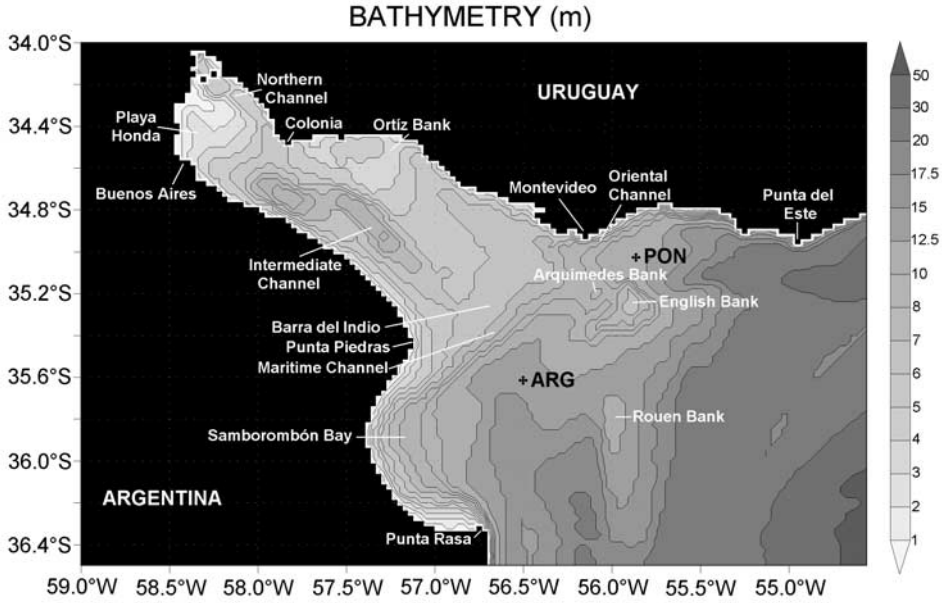

Figure 1. Bathymetry (in meters) of the study area as it derives from a 3 km × 3 km resolution data set together with the main geographical and topographical features. Locations where ADCP time series were collected are indicated as PON and ARG.

what is known about its behavior was inferred from numerical simulations. Maximum speeds seem to occur at the northernmost and southernmost limits of Samborombón Bay (Punta Piedras and Punta Rasa) while in its interior, values are much smaller. This last region displays a rotational feature, but at the upper and central estuary the currents tend to be more unidirectional; this last is also the case along the Uruguayan coast [*Simionato et al.*, 2004a].

[4] Owing to the large discharge, the estuary forms, when it meets the ocean, an intense and active salinity front followed by a fresh water plume whose influence can be tracked as far as 23°S [*Campos et al.*, 1999]. They are not only important for fisheries [*Cousseau*, 1985; *Boschi*, 1988; *Bava*, 2004], but also modify the coastal circulation and the mixing and convection conditions [*Piola et al.*, 2000] with important oceanographic implications. The processes associated with the interaction of fresh river water and saline shelf water and tidal stirring generate a turbidity front which is tied to the bottom salinity front [*Framiñan and Brown*, 1996].

[5] The characteristics of the salinity front have been described by *Guerrero et al.* [1997] and *Framiñan et al.* [1999], and its dynamics in the seasonal scale have been modeled by *Simionato et al.* [2001]. The temporal variations of the turbidity front were studied by *Framiñan and Brown* [1996] and *Bava* [2004]. These papers show that the surface salinity front position presents intense variability in subannual, seasonal, and interannual timescales. In the seasonal scale, during fall-winter, as a consequence of the rotation of the Earth and a minimum in the wind speed, the fresh water plume moves north-northeastward following the Uruguayan (northern) coast [see, e.g., *Guerrero et al.*, 1997, Figure 4]. In spring-summer, mean winds are more intense and blow westward; as a result, the fresh water plume displaces southwestward and moves following the Argentinean (southern) coast [see, e.g., *Guerrero et al.*, 1997, Figure 5]. In the interannual timescale, large variations of the frontal position have been mainly related to variability in the runoff [*Framiñan and Brown*, 1996; *Mianzan et al.*, 2001]. In shorter timescales, large excursions of the frontal position are known to occur [*Framiñan and Brown*, 1996; *Bava*, 2004]. Both data and model simulations suggest the wind as the main forcing of the estuarine dynamics [*Framiñan and Brown*, 1996; *Simionato et al.*, 2004b]; given the large wind variability observed in the area [*Simionato et al.*, 2005], it is expected that in the synoptic scale, large excursions occur in the surface front.

[6] The bottom salinity front, in opposition, shows a more stable position throughout the year. The continental shelf water intrusion from the bottom to the estuary is controlled by the bathymetry, the bottom front remaining located, approximately, following the 10-m isobath [*Guerrero et al.*, 1997]. As a result of the bottom front steadiness and the surface front extension and constant displacement, the estuary exhibits a time-variable salt wedge structure that is observed during most of the year. The main features of this salt wedge have been described by *Guerrero et al.* [1997] and *Framiñan et al.* [1999]. These authors showed that the horizontal extension and vertical gradient of this salt wedge suffers a seasonal cycle related to the surface salinity front displacements. This way, whereas the salt wedge is a semipermanent feature of the central and southern portions of the estuary, this structure can be lost during summer along the northern portion as a result of the southwestward retraction of the surface salinity front. The salt wedge has a mean horizontal extension of around 150 km in the northern and 100 km in the central and southern portions of the estuary during winter, whereas in summer the extension in the southern part can reach 250 km [see *Guerrero et al.*,

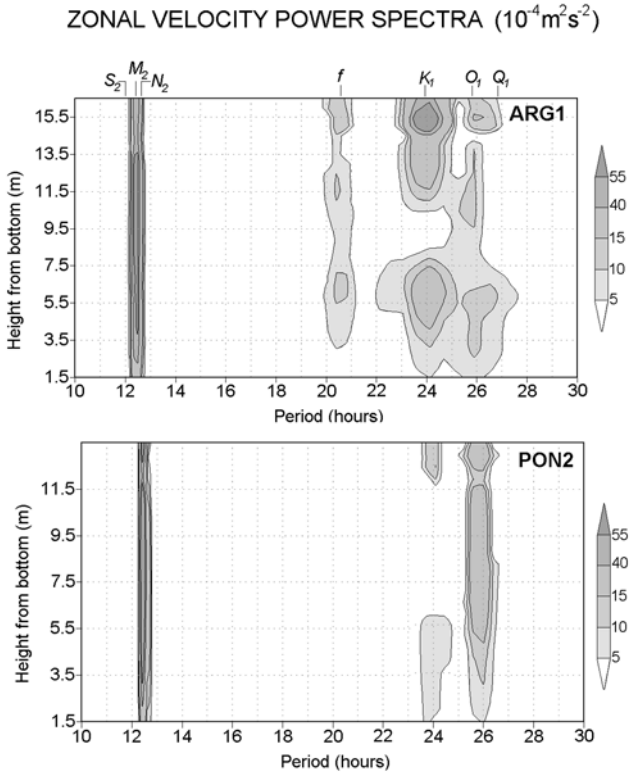

Figure 2. Vertical distribution of the spectral variance of the zonal velocity component of (top) ARG1 and (bottom) PON2. Units are in 10^{-4} m^2 s^{-2}. Only contours significant to a 99% confidence level have been plotted. Periods corresponding to the most important tidal constituents and the inertial period have been highlighted.

1997, Figures 8 and 9]. Observations indicate that vertical gradients as large as almost 16 psu m^{-1} can exist in the region in winter, but they are reduced to maximum values of around 8 psu m^{-1} during summer [*Guerrero et al.*, 1997]. Even though the salt wedge can be destroyed under persistent moderate to intense winds with a southerly component [see *Guerrero et al.*, 1997, Figure 10], it seems to be rapidly regenerated afterward, given that it characterizes the seasonal mean pattern.

[7] These two-layer characteristics make the estuary an adequate environment for the generation of internal waves during long periods of the year. Tidal-frequency oscillations with characteristics of baroclinic waves have been observed by *Dragani et al.* [2002] and *Sepúlveda et al.* [2004] from ADCP transects collected in the estuary. These authors have found intense vertical variability in the velocity in these frequencies, showing reversions of the current direction between the upper and lower layers. Nevertheless, their studies were limited by the shortness of the records that in both cases was 24 hours. Given that intermittency is one of the main features of internal oscillations, long records are necessary for their proper analysis. Recently, in the frame of the UNDP/GEF Project "Environmental Protection of the Río de la Plata and its Maritime Front" (FREPLATA), relatively long period ADCP current series with high vertical and temporal resolution were collected at two locations of the estuaries' frontal zone: the Maritime Channel, proximate to Argentinean coast, and Pontón Recalada, close to Montevideo, on the Uruguayan coast. These data provide the first opportunity for analyzing the vertical structure of the currents in tidal frequencies in the region. The aim of this paper is, therefore, to study the current oscillations in periods less than 30 hours in these locations in an attempt to characterize the barotropic tidal and mean currents and the internal oscillations present in the records.

2. Data

[8] In the frame of the UNDP/GEF FREPLATA Project, current vertical profiles were measured at two locations in the Río de la Plata estuary. Initially, the project involved the simultaneous collection of data in the Maritime (Argentinean side) and Oriental (Uruguayan side) channels through the use of two RDI Acoustic Doppler Current Profilers (ADCP) of 1200 and 600 MHz, respectively. Each ADCP was located in a stainless steel mooring, which was linked to a weight of 5 tons by means of steeling cable. The weight was marked by a superficial buoy. The ensemble interval was set to 10 min, with 150 pings per ensemble, and the vertical resolution to 0.5 m. The compass was calibrated before the deployment. After almost 3 months, during the first retrieving data task in the Uruguayan side, it was detected that the cable had been cut and, consequently, the 600-MHz ADCP had been lost.

[9] The ADCP on Argentinean side, moored at 35°40′S, 56°30′W at a depth of 17 m, is referred to as ARG in Figure 1. It was recovered, data were retrieved, and the instrument was deployed again, completing a total sampling period of more than 6 months. This way, two series (hereinafter referred to as ARG1 and ARG2) were obtained at that location spanning the periods 4 December 2002 to 21 February 2003 and 22 February to 5 June 2003, respectively, with 31 levels each. Afterward, this instrument was moored again in September 2003 on the Uruguayan side very close to Pontón Recalada, at 35°02′S, 55°51′W, and pointed out as PON in Figure 1. The depth in this location is 15 m. Two series (hereinafter referred to as PON1 and PON2) with a total of 27 levels each were obtained, spanning the periods 3 September to 13 November 2003 and 14 November 2003 to 26 March 2004, respectively.

[10] A careful quality control of every time series was done. A few gaps, probably due to larger than normal reductions in the water level, were observed in the first two layers. Immediately after and before these gaps, spurious values (differences in consecutive values larger than 2 standard deviations) of the speed usually appeared, which were eliminated from the records. As a result, a small number of data (less than 1%) were filled by lineal interpolation between adjacent accepted data in the first two layers.

3. Results

[11] To provide a first view of the energy distribution in the different tidal periods, power spectra of the zonal and meridional current components were computed for every time series at every vertical level and plotted in z versus period diagrams. As an example, Figure 2 shows the results obtained for the zonal velocity component of ARG1

Table 1. Results of a Variance Analysis for the Barotropic and Baroclinic Components of the Currents Observed in ARG and PON for High Frequencies (Periods Less Than 30 Hours)

	High Frequencies Energy (Percentage of the Total Variance), $m^2\ s^{-2}$	Barotropic High Frequencies Energy, %	Baroclinic High Frequencies Energy, %
	ARG1		
u	3.48 (65%)	51	49
v	4.06 (46%)	59	41
	ARG2		
u	2.98 (55%)	63	37
v	3.06 (41%)	64	36
	PON1		
u	4.17 (44%)	76	24
v	1.34 (31%)	33	67
	PON2		
u	4.37 (43%)	74	26
v	1.53 (35%)	36	64

(Figure 2, top) and PON2 (Figure 2, bottom). Results for the meridional component display very similar features and, therefore, are not shown. Note that in the figure, only those contours significant to a 99% confidence level were drawn. The periods of the most important tidal constituents in the region (M_2, S_2, N_2, K_1, O_1, and Q_1) as well as the inertial period (*f*) have been highlighted in the figure. Figure 2 (top) indicates that in ARG1, in periods lower than 30 hours, wave activity is present in the semidiurnal band, the diurnal band, and the inertial period (which is 20.58 hours at this latitude). No significant peaks were detected in periods lower than 10 hours. One interesting feature emerging from Figure 2 is that activity in the 24-hour period displays a vertical structure and is as energetic as activity in the M_2 and O_1 bands, particularly in the upper layers. M_2 is, by far, the most important tidal constituent in the area, and it is also known that O_1 and K_1 are of the same order of magnitude [*D'Onofrio et al.*, 1999]. Therefore the structure observed in the spectra could be an indication of the existence of baroclinic wave activity in the diurnal band. Variance in the inertial period also displays a vertical structure, with maxima at the uppermost level and at around 6.5 m from the bottom. This suggests the presence of waves with an internal structure in this band as well. Even though the signals at the inertial period and the diurnal band were less energetic in ARG2, similar results were obtained in the other bands.

[12] In PON2, as revealed by Figure 2 (bottom), even though there are wave activity signatures in the main tidal frequencies, the signal in the inertial period is absent. Indication of baroclinic wave occurrence in the diurnal band is also apparent in this figure. In this case, energy in the O_1 band dominates the diurnal band of the spectra. Nevertheless it must be taken into account that in this location, O_1 is the dominant diurnal constituent, being approximately twice as energetic as K_1.

[13] To evaluate the relative contribution to the total energy of the barotropic and baroclinic motions in the different frequencies and locations, a variance analysis was performed. First, a 907-element high-pass filter with a cutoff period of 30 hours was applied to the time series. Then the barotropic component of the filtered time series was computed as the vertical mean and subtracted from the data in order to obtain the baroclinic (vertically varying) component. The variance of each of the thus obtained time series was computed and the percentages of total variance accounted for by their barotropic and baroclinic components were calculated. Results are shown in Table 1, where values represent the vertically averaged variance or kinetic energy per mass unit, in $m^2\ s^{-2}$.

[14] The first feature emerging from Table 1 is that in all the cases the amount of total energy in the high frequencies is comparable to the one in the low frequencies. On occasion, like in ARG1 and ARG2, high frequencies account for more than 50% of the total variance of the zonal velocity component. The barotropic/baroclinic energy partition reveals, nonetheless, that this is not only the result of intense tidal barotropic motions in that band of frequencies but also the result of energetic baroclinic oscillations. These last have variances that, on occasion, can be as large as those due to the barotropic motions. This is the case, for example, in ARG1, where the baroclinic component accounts for 49 and 41% of the total variance of the zonal and meridional velocity components, respectively. Another interesting feature is the difference in the relative importance of the barotropic/baroclinic velocity from one to another sampling period and location. For example, energy due to baroclinic zonal velocity component, which accounts for almost 50% of the variance in ARG1, only explains 37% in ARG2, and around 25% in PON1 and PON2. Given that, except for the tides, the estuary response depends upon time varying forcings, such as the river discharge and winds, and the time varying vertical density structure, that result reflects the high variability that characterizes the region.

[15] On the basis of the above results, it was decided to study separately the barotropic and baroclinic signals in periods lower than 30 hours. Results of these analyses are discussed in what follows.

3.1. Barotropic Signal

[16] The barotropic velocity analyzed in what follows was obtained by computing the instantaneous vertical mean of the original 10-min sampling period records. The thus resulting time series were analyzed for tidal currents applying *Foreman*'s [1978] technique. Following this author, three consecutive moving average filters of order 6, 6, and 7 respectively, were applied to the time series prior to the harmonic analysis. The Rayleigh criterion was used to determine the number of constituents to be included.

[17] Similar values characterizing tidal ellipses were obtained from the analyses of ARG1 and ARG2. This result is consistent with the fact that both records are of similar length. Therefore an average between them was considered as a representative result. In the case of PON1 and PON2, nevertheless, probably owing to the fact that the first series is much shorter than the second one, differences were obtained in the smaller amplitude constituents between both records analyses. In this case, results corresponding to the longest series, PON2, that can be considered more accurate, will be shown.

[18] Tidal ellipses as derived from these calculations are shown in Figures 3 (for ARG) and 4 (for PON). Note that

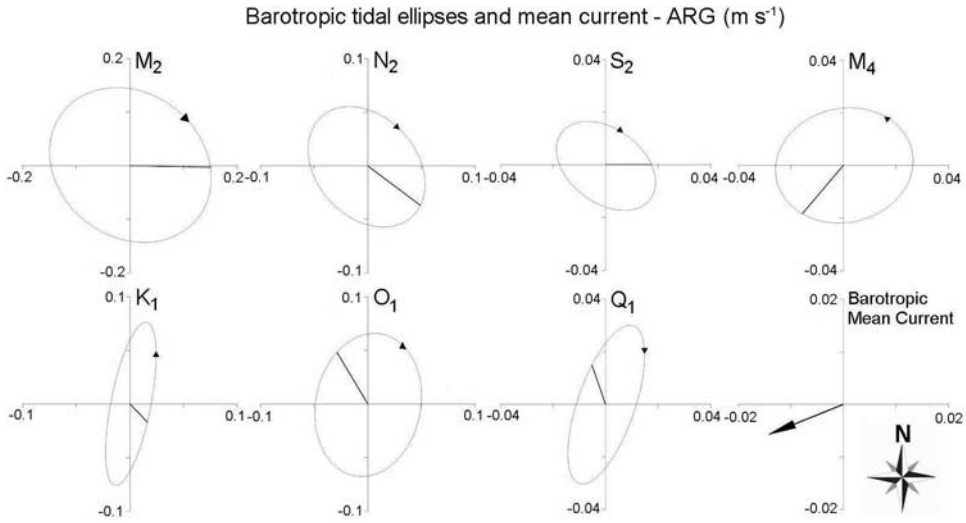

Figure 3. Velocity ellipses corresponding to M_2, N_2, S_2, M_4, K_1, O_1, and Q_1 tidal constituents and barotropic mean current as derived from the data collected in ARG. Results were obtained as an average between harmonic constants in ARG1 and ARG2. Note that different scales have been used for the different constituents. Arrows represent the sense of rotation, and solid lines represent the Greenwich phase.

the scales of the plots are different for the diverse constituents. It comes out from Figures 3 and 4 that in both, ARG and PON, M_2 is the most important tidal constituent; this is in good agreement with observations [*D'Onofrio et al.*, 1999]. Consistent with what derives from numerical simulations [*Simionato et al.*, 2004a], in ARG the M_2 tidal ellipse (Figure 3, top left) has a clockwise rotation and a west-northwest to east-southeast orientation. Similar characteristics are shown by the other semidiurnal constituents, such as N_2 and S_2 (Figure 3, top center). In PON the semidiurnal constituents (Figure 4) are very elongated, with an east-west orientation, and M_2 has a counterclockwise rotation. These characteristics are also consistent with what is known about tides in the region and with numerical simulations of tidal propagation in the area [*Simionato et al.*, 2004a]. In both locations the diurnal constituents O_1, K_1, and Q_1 significantly contribute to tidal currents in that order of importance. Noticeably, in all the records, the tidal current in the M_4 frequency (Figures 3 and 4, top right)

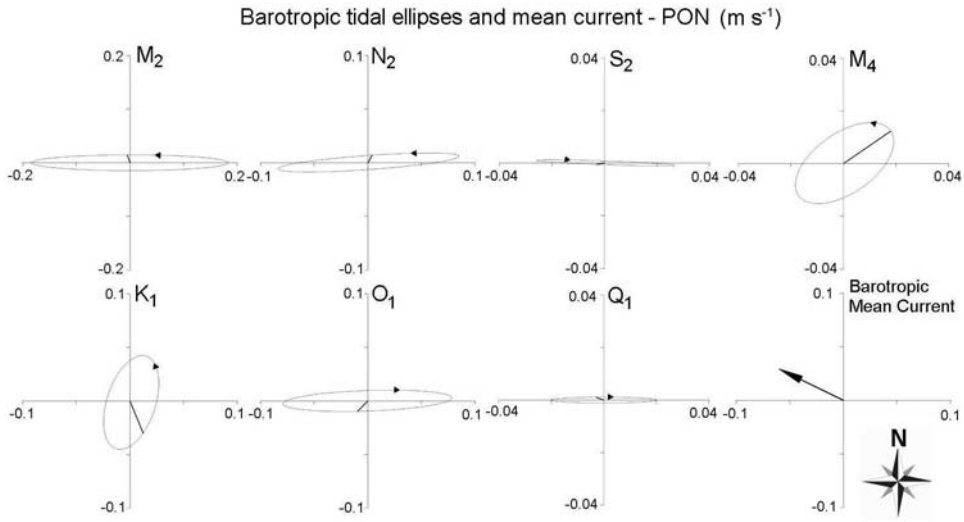

Figure 4. Velocity ellipses corresponding to M_2, N_2, S_2, M_4, K_1, O_1, and Q_1 tidal constituents and barotropic mean current as derived from the data collected in PON2. Note that different scales have been used for the different constituents. Arrows represent the sense of rotation, and solid lines represent the Greenwich phase.

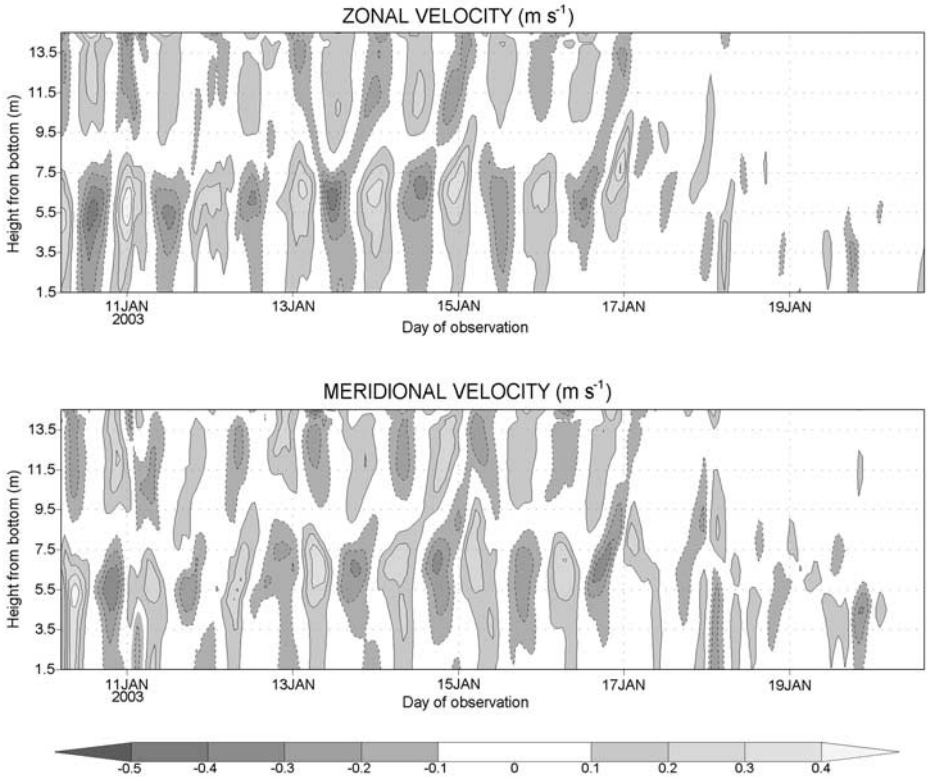

Figure 5. The *z-t* Hovmöller diagrams for the (top) zonal and (bottom) meridional current components in ARG between 10 and 21 January 2003. Contour interval is 0.1 m s^{-1}, and only speeds larger that 0.1 m s^{-1} have been contoured.

is comparable to the one related to Q_1 or S_2, suggesting that nonlinear interaction is an important feature in the area.

[19] The residual barotropic mean current (Figures 3 and 4, bottom right) shows, in both locations, different speeds and directions, which in every case are consistent with the seasonal excursion of the fresh water plume shown by historical salinity data [*Guerrero et al.*, 1997]. In summer, the fresh water plume suffers a retraction to the southwest, forced by the easterly dominant winds, whereas during winter, owing to the low magnitude of the mean winds, it extends northward along the Uruguayan coast deviated by the Coriolis force, acting to the left in the Southern Hemisphere [*Simionato et al.*, 2001]. During spring, mean winds have features resembling the summer situation, even though weaker [*Simionato et al.*, 2005]; therefore during this season a behavior of the plume similar to the one observed in summer occurs [*Guerrero et al.*, 1997]. Fall is a transition season with a distinctive mean wind pattern [*Simionato et al.*, 2005]; during this season, climatology indicates that the fresh water plume begins to develop the northward excursion that characterizes the cold season [*Guerrero et al.*, 1997]. Consistently, in ARG, where data were collected during summer and fall, the mean barotropic current direction (Figure 3, bottom right) is to the west-southwest and its magnitude is low, 0.016 ± 0.004 m s^{-1}; this is expected to result from the combination of an intense summer retraction to the southwest of the fresh water plume and a relatively weak autumn extension of this feature to the north. In PON (Figure 4, bottom right), where data were acquired during spring/summer, mean barotropic velocity is to the west-northwest, but its speed is larger, with a value of 0.058 ± 0.004 m s^{-1}, consistent with the warm season frontal retraction.

[20] Finally, it is worthwhile to point out that in both locations, tidal and mean barotropic currents account for approximately 90% of the variance of the barotropic signal in periods less than 30 hours. No clear periodicity was observed in the residual signal in any of the records. The fact that inertial oscillations were not observed in the barotropic velocity is an indication that at least the wave detected in ARG in that frequency (Figure 2) is not of barotropic nature and must be, therefore, a baroclinic oscillation.

3.2. Baroclinic Signal

[21] To extract the baroclinic signal in tidal frequencies, the instantaneous vertical mean current was subtracted to the (30-hour cutoff period) high-pass filtered data. These differences, consequently, represent the baroclinic velocity component in periods of oscillation less than 30 hours. A portion of *z-t* Hovmöller diagrams of the thus obtained zonal (u) and meridional (v) baroclinic velocity components for ARG1 are shown in Figure 5. Here a pattern consistent with baroclinic wave's activity is clearly visible. Between 10 and 17 January, both velocity components are charac-

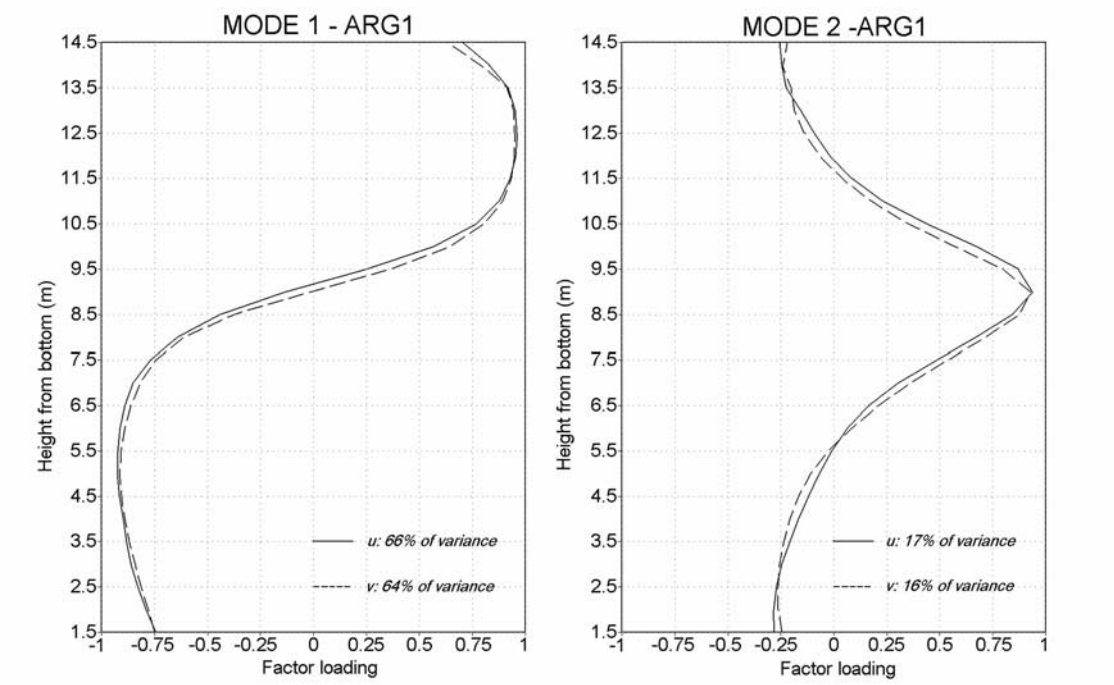

Figure 6. Vertical structure of the (left) first and (right) second modes derived from the Principal Components analysis of the zonal (solid line) and meridional (dashed line) baroclinic currents in ARG1.

terized by a vertical structure with a sign reversal between the upper and lower layers, oscillating within a period of around 24 hours. Velocities as high as 0.5 m s^{-1} are related to these waves. A phase lag is observed between oscillations in the zonal and meridional directions, indicating a counterclockwise rotation. The lack of wave signal after 17 January is typical of the intermittency that characterizes internal wave activity. Similar features can be observed in other lapses of time in both this location and PON.

[22] To extract the vertical structure that characterizes the energetic internal waves detected, a Principal Components (EOF) analysis was applied to the time-vertically varying *u* and *v* data. The analysis was applied independently to both velocity components, and the data of the two uppermost meters, noisy and more affected by surface wind waves, were kept out of it. From the results for the time series collected in ARG, it emerges that two modes, accounting together for more than 80% of the variance, are related to a pattern distinctive of internal wave's activity. Figure 6 shows the vertical structure of those modes for ARG1. Mode 1 of the zonal and meridional velocity components (Figure 6, left), accounting approximately for 65% of the variance, displays a vertical structure with a sign reversal between the upper and lower portions of the water column, characteristic of internal waves. The maximum vertical gradient is located between 8.5 and 9.5 m from the bottom. Mode 1 structure is almost identical for both components and both sampling periods, ARG1 (Figure 6) and ARG2 (not shown). Power spectra of the time series related to these modes reveals that this structure is associated with oscillations of similar periods in ARG1 and ARG2. In ARG1 (Figure 7, top), main peaks are found in bands centered at approximately 24 hours and the inertial period. A weak, even significant peak is found in the *v* Mode 1 spectra at the semidiurnal period; this peak is marginal for *u* Mode 1. A cross-spectral analysis between time series of modes 1 for *u* and *v* (Figure 7, bottom) indicates that oscillations for both velocity components are highly coherent in the diurnal and inertial periods. The phase lag is of around 90° and 100° for waves in these bands, respectively, *u* leading *v*. This is consistent with counterclockwise rotation in both cases. The similar amplitude of the peaks in the *u* and *v* spectra at the inertial period (Figure 7, top) and the phase lag between them (Figure 7, bottom right) are reasonably consistent with inertial oscillations. In ARG2 (not shown), even though the percentage of variance explained by *u* and *v* first modes is similar, the peaks in the diurnal band are of smaller amplitude than those obtained for ARG1. Consistently, baroclinic energy of ARG2 (Table 1) is smaller than that of ARG1.

[23] Second mode (shown for ARG1 in Figure 6, right) accounts for more than 15% of the variance of *u* and *v* in both, ARG1 and ARG2. Even though modes are similar for both velocity components and preserve their pattern from one to another sampling period (ARG1 in Figure 6, and ARG2, not shown), they do not exhibit clear periodicities in the band of frequencies considered in this study. Vertical structure of this mode is consistent with differences in the internal waves from one to another event owing to variations in the vertical location of the pycnocline.

[24] In order to identify the periods of waves occurrence, a wavelet transform was applied to the time series of modes 1 derived from the EOF analysis, which extract the wave signature. Following *Torrence and Compo* [1998], a Morlet mother wavelet function with a parameter of 6 was chosen. Amplitude scaleograms resulting from the ARG1 and ARG2 *u* Mode 1 time series are shown in Figure 8, where only those values significant to a 99% confidence

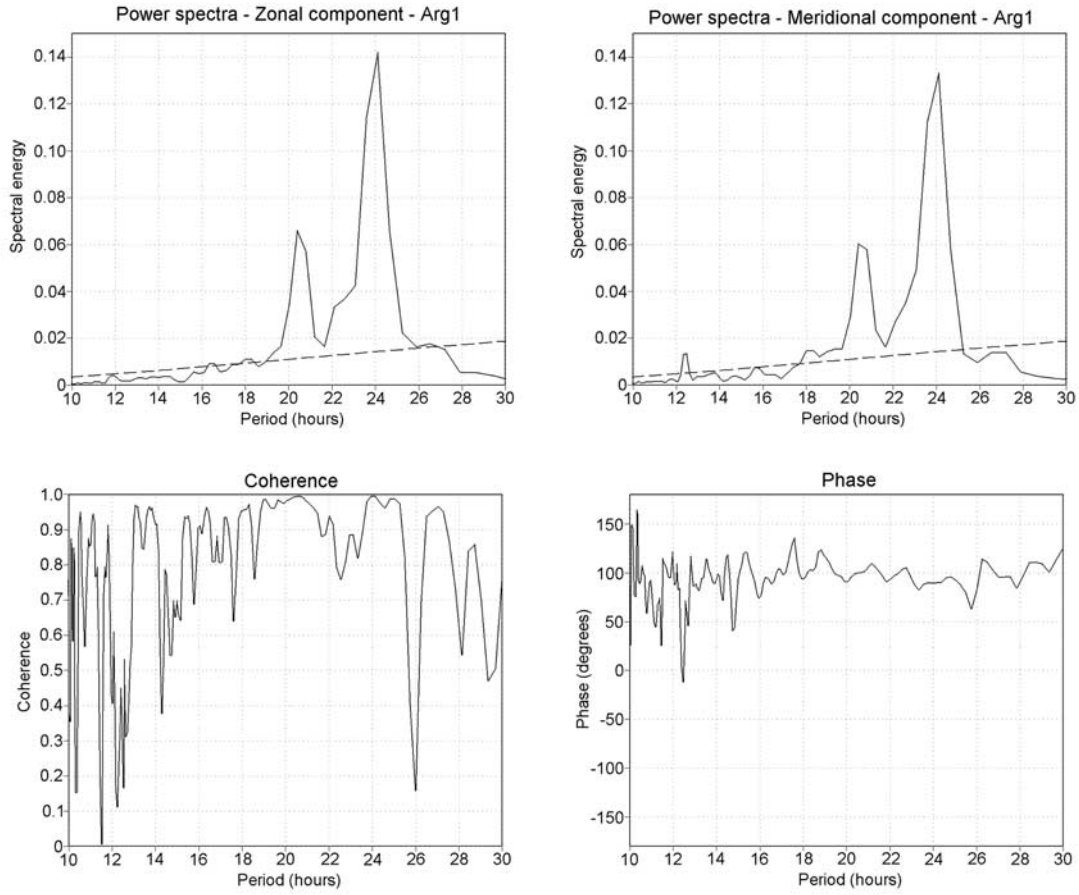

Figure 7. (top) Power spectra of the time series related to the modes 1 resulting from the Principal Components analysis of the (left) zonal and (right) meridional current components in ARG1; dashed line indicates the 99% confidence level. (bottom) (left) Coherence and (right) phase lag derived from a cross-spectral analysis between u and v modes time series.

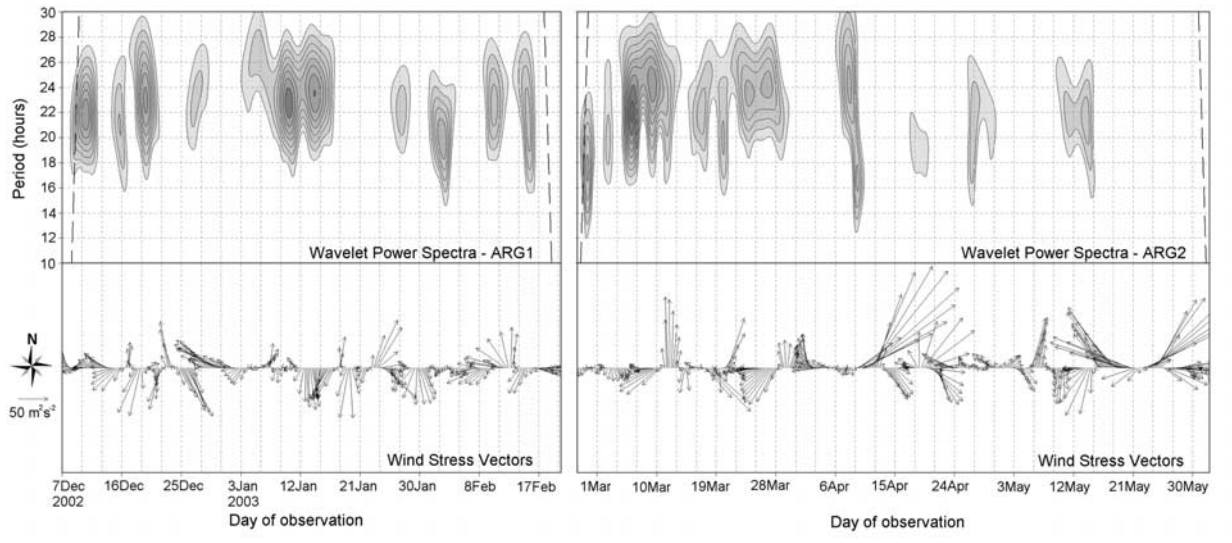

Figure 8. (top) Amplitude scaleograms of the zonal velocity component modes 1 time series in ARG1 and ARG2. Only contours significant to a 99% confidence level have been plotted. Vertical lines at the beginning and ending of the plots define the cone of influence. (bottom) Wind stress vectors as derived from the NCEP/NCAR reanalyses with a 6-hour temporal resolution.

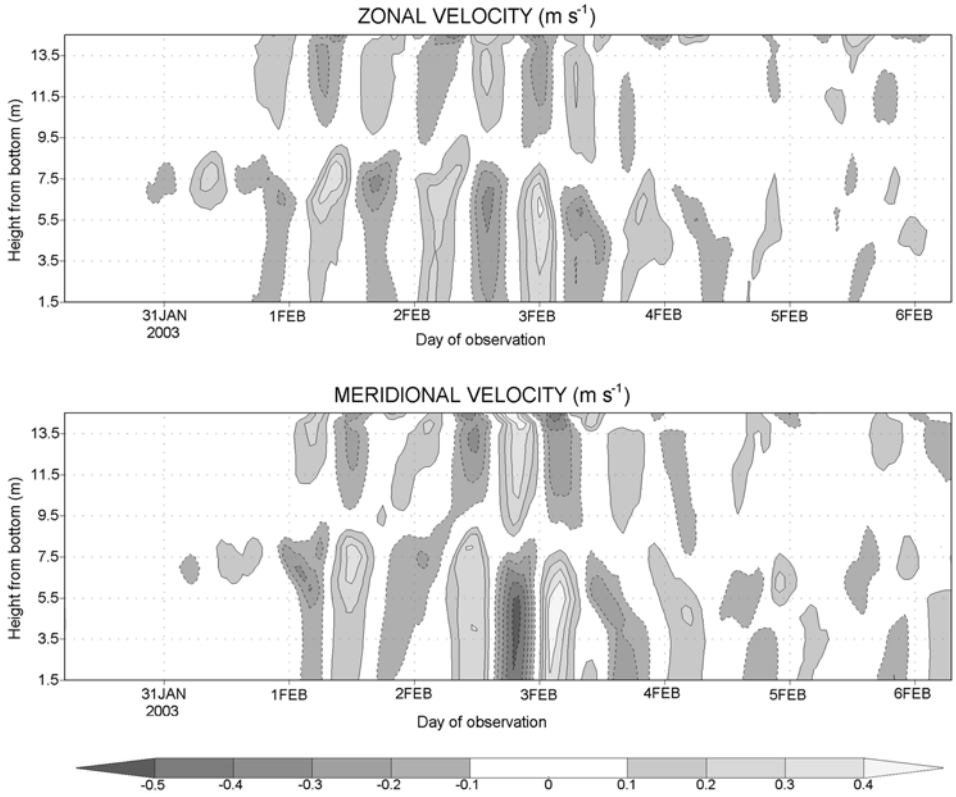

Figure 9. The *z-t* Hovmöller diagrams for the (top) zonal and (bottom) meridional current component in ARG between 30 January and 6 February 2003. Contour interval is 0.1 m s^{-1}, and only speeds larger that 0.1 m s^{-1} have been contoured.

level were contoured. Dashed lines at the beginning and end of the plots represent the cone of influence, outside which the analyses results can be misleading. Scaleograms derived from the meridional velocity components (not shown) exhibit almost identical characteristics. This is consistent with the EOF and cross-spectral analyses which indicate, respectively, a similar vertical structure and variance for the peaks of both velocity components in every time series in this location.

[25] It can be seen in Figure 8 that internal waves with periods between the inertial and diurnal are often active in ARG during the sampled period. Events are very frequent during the ARG1 sampling period where, individually, they seem to last for around 3 days. In ARG2, even though there is intense activity during March, it considerably decays as the Southern Hemisphere autumn goes by. In effect, only one intense event centered on 8 April, and two weak ones, occurring around 28 April and 14 May, can be observed during the fall sampled months.

[26] A sequence of intense events with periods around 24 hours can be observed during the first half of January 2003; they coincide, in part, with the lapse of time shown in the Hovmöller diagrams of the observed baroclinic velocity in Figure 5. An event with shorter period, around the inertial one, can be identified during the first days of February 2003. Hovmöller diagrams of the observed zonal and meridional baroclinic velocity components for this period are shown in Figure 9. Here an internal wave can be observed being excited during the last hours of 31 January, reaching its maximum intensity 48 hours later and lasting, in total, approximately 72 hours. The lack of signal prior to and after the waves is consistent in both the scaleogram derived from the *u* EOF Mode 1 (Figure 8) and the Hovmöller diagrams derived from the velocity data (Figures 5 and 9), not only for these but also for all the other periods when wave activity is indicated by the wavelet decomposition. This indicates that the statistical methodology applied is consistent and useful in identifying waves.

[27] A similar analysis was applied to PON data. Results indicate some interesting differences between both locations. Figure 10 shows the vertical structure of the first and second modes derived from the Principal Components analysis of the zonal and meridional baroclinic velocity components (excluding the uppermost 2 m) of PON2. Results from PON1 are very similar and, therefore, are not shown. It can be seen in Figure 10 that in this location, even though the percentage of variance accounted for by both modes is very similar to the one obtained for ARG (Figure 6), the methodology cannot extract an identical vertical pattern for *u* and *v*. Nevertheless, a wavelike structure is still evident in Mode 1, with a sign reversal between the uppermost and lowermost levels; Mode 2, once more, is consistent with variations in waves due to changes in the pycnocline position. The maximum vertical gradient is located, in this case, between 6.5 and 7.5 m from the bottom. The difference observed between the modes related to *u* and *v*

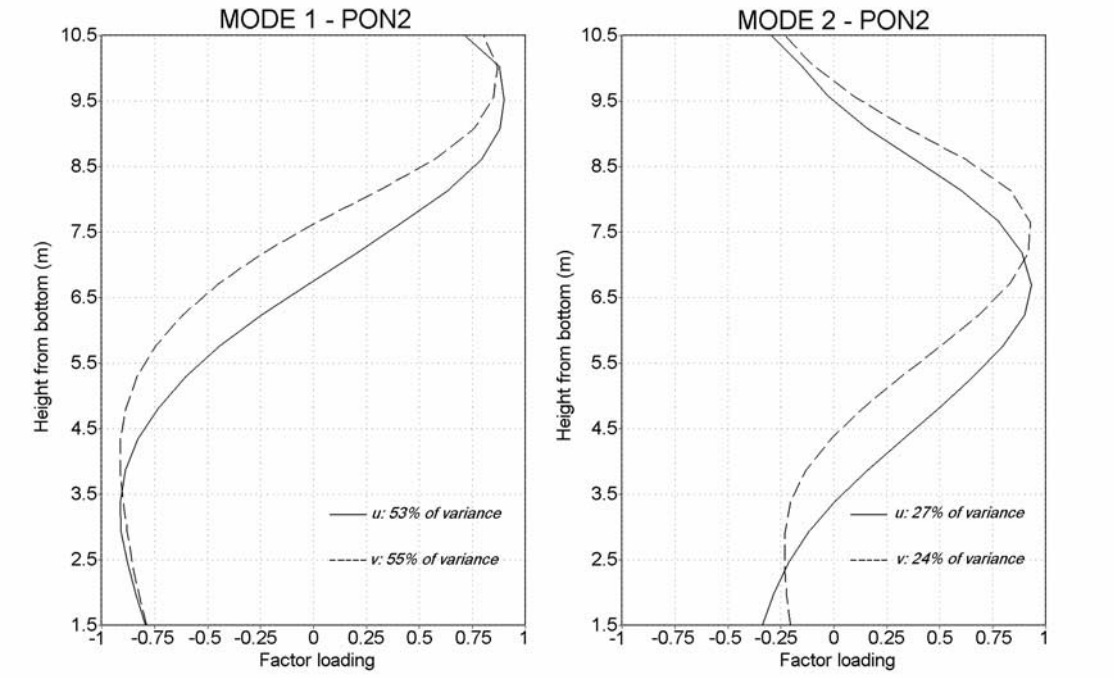

Figure 10. Vertical structure of the (left) first and (right) second modes derived from the Principal Components analysis of the zonal (solid line) and meridional (dashed line) baroclinic currents in PON2.

can be understood looking at the results of the spectral analyses of the time series of modes 1. In both PON2 (Figure 11) and PON1 (not shown), energy peaks around the semidiurnal and diurnal bands were found in the power spectra of the zonal component Mode 1 (Figure 11, top left). Nevertheless, in the meridional component, only one peak in the diurnal band was detected (Figure 11, top right). The signal in the diurnal band is coherent between u and v modes 1 with a phase lag of around 100° between them (Figure 11, bottom panels). Similarly to ARG, u leads v, indicating a counterclockwise rotation. Signal is more energetic in the meridional than in the zonal component. Results from PON1 (not shown) indicate that even though the peak at the semidiurnal band is of the same amplitude as in PON2, the one in the diurnal band is of smaller amplitude.

[28] Results from the wavelet decomposition of the time series of EOF u modes 1 in this location are shown in Figure 12. Wave activity can be observed all along the record. Similarly to ARG, events with frequencies in the diurnal band seem to have in general a length of around 3 days, even though a few shorter and weaker events can also be observed. In periods around the semidiurnal, wave activity can be seen, for example, by the middle of October, the end of November, the end of December, and the middle of January. No relation between the periods of occurrence of this wave activity and the moon phases is observed. Consistent with the spectral analysis of Figure 11, these last signals are not present in the v Mode 1 wavelet decomposition (not shown). As an example, z-t Hovmöller diagrams of u and v baroclinic velocity data collected between 15 and 22 January are shown in Figure 13. In good agreement with wavelet analysis results, an internal wave event with a period of around 12 hours can be observed between 17 and 19 January. The wave signature is mainly related to the zonal velocity component.

3.3. Discussion

[29] Analyses of data collected at two different locations of the frontal zone of the Río de la Plata estuary led to results consistent with intermittent internal wave's activity, with periods around the semidiurnal and the inertial to diurnal. Linear theory indicates that internal waves cannot exist as freely propagating modes for frequencies lower than the inertial [*Gill*, 1982]. Therefore the observed waves with period around 24 hours must be forced, steady ones.

[30] The occurrence of internal waves depends on the availability of an appropriate environment and of a forcing to excite them. Unfortunately, there are no temperature and salinity time series simultaneous to our velocity observations to make an evaluation of the stratification variability and its relation to the observed waves. In the Río de la Plata estuary, as the bottom fresh water is trapped by the bathymetry at the 10-m isobath [*Guerrero et al.*, 1997], the salt wedge variability is essentially dominated by the upper fresh water layer behavior. This, in turn, basically results from an equilibrium between the fresh water discharge and the winds. Given the large runoff, its long temporal scale of variability [*Jaime et al.*, 2002], the broadness of the estuary, and the location where oscillations were observed, it seems unlikely that variations in the discharge play a fundamental role in controlling the vertical structure and, therefore, the waves' generation in short timescales. Consequently, it seems natural to consider the winds as the main source of variability in this temporal scale in the area.

[31] Wind data were used to help build hypotheses about the causes of the observed variability in the occurrence of

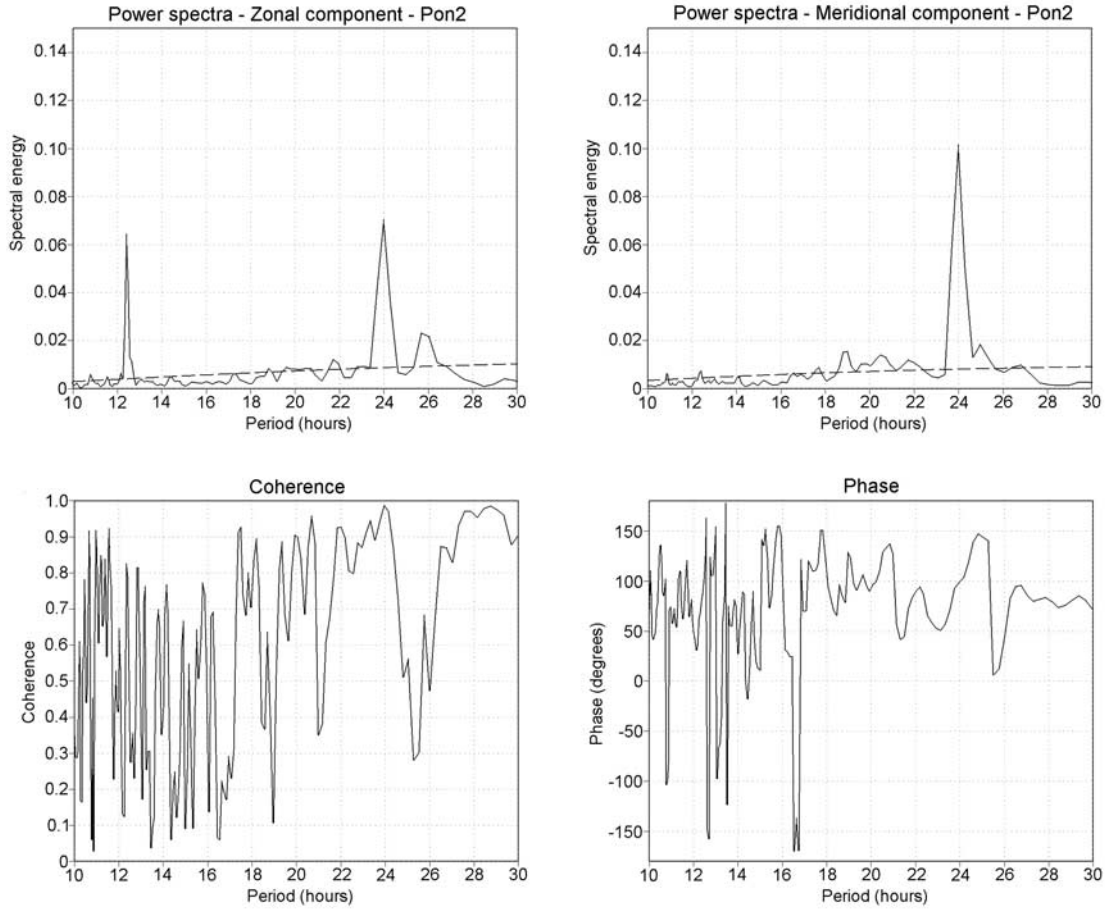

Figure 11. (top) Power spectra of the time series related to the modes 1 resulting from the Principal Components analysis of the (left) zonal and (right) meridional current components in PON2; dashed line indicates the 99% confidence level. (bottom) (left) Coherence and (right) phase lag derived from a cross-spectral analysis between the modes time series.

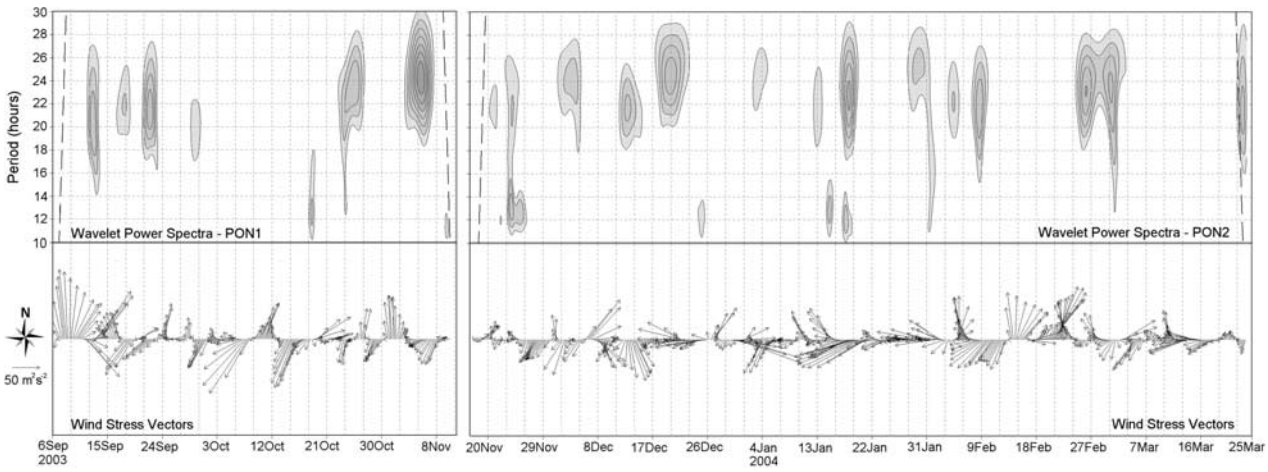

Figure 12. (top) Amplitude scaleograms of the zonal velocity component modes 1 time series in PON1 and PON2. Only contours significant to a 99% confidence level have been plotted. Vertical lines at the beginning and ending of the plots define the cone of influence. (bottom) Wind stress vectors as derived from the NCEP/NCAR reanalyses with a 6-hour temporal resolution.

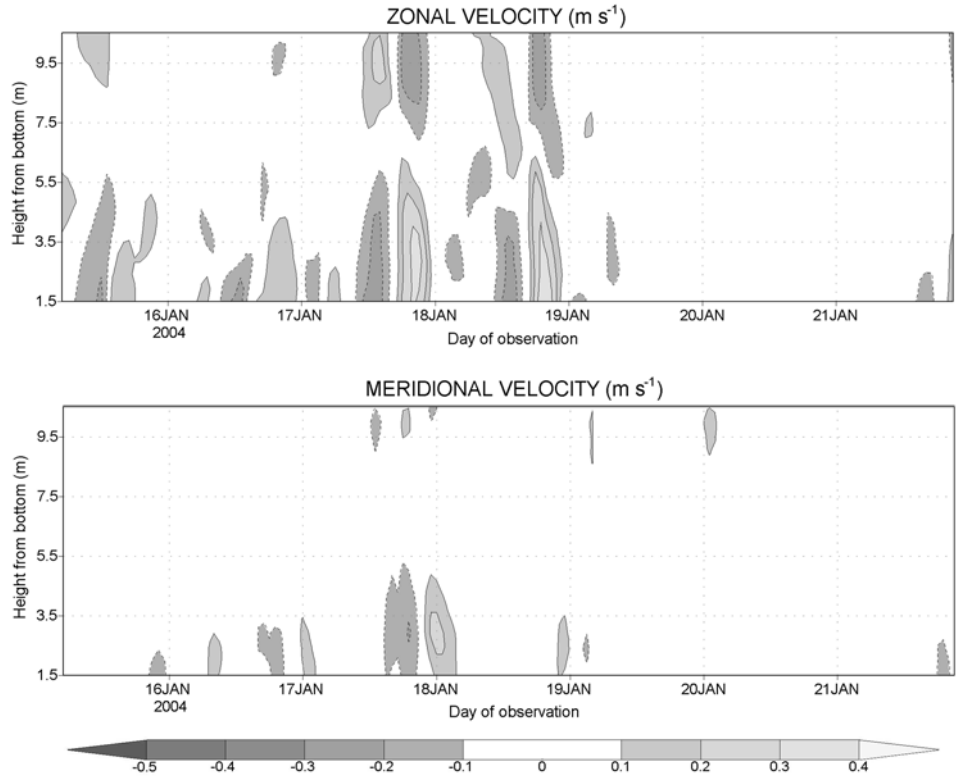

Figure 13. The *z-t* Hovmöller diagrams for the (top) zonal and (bottom) meridional current component in PON between 12 and 20 January 2003. Contour interval is 0.1 m s^{-1}, and only speeds larger that 0.1 m s^{-1} have been contoured.

internal waves. Some portable rotating-cup anemometer observations were collected in Pontón Recalada station (very close to PON) simultaneously with the ADCP data studied in this paper. Unfortunately, they do not have constant sampling interval, and there are a number of gaps with no observations at all that seriously limit the use of these data. Therefore a comparison of those observations with the twice-daily scatterometer data collected by the SeaWinds instrument on the QuikSCAT satellite (http://podaac.jpl.nasa.gov/quikscat) and the 4-daily data derived from the NCEP/NCAR reanalyzes (http://www.cdc.noaa.gov) was done, in order to identify a suitable source of alternative atmospheric data. When comparing, the different characteristics of the diverse data sets must be taken into account. Pontón Recalada observations are direct and close to PON; therefore, even though they probably are not very accurate, they must be considered the best data when available. Scatterometer data are instantaneous observations of the backscatter of the ocean and are converted to wind speed and direction through mathematical algorithms [*Naderi et al.*, 1991; *Wu et al.*, 1994]; usually it is not considered convenient to use these data when they are very proximate to the coast. The error of the observations is 2 m s^{-1} in the speed and 20° in the direction; the spatial resolution is very high, 25 km. The sampling period is 24 hours in two passes, the ascending pass (6AM LST equator crossing) and descending pass (6PM LST equator crossing). NCEP/NCAR reanalyses are not direct observations but the result of an objective analysis combining rawinsonde observations around the world, remote observations collected via satellite-borne instruments, and a physical numerical model [*Kalnay et al.*, 1996]. The result of this analysis is a set of gridded data with a spatial resolution of 2.5° (approximately 250 km) and a temporal resolution of 6 hours. The main advantages of these reanalyses are their physical consistency and relatively high temporal resolution.

[32] Figure 14 shows the wind vectors derived from these three sources for January 2003. Beyond the differences in the sampling intervals, two characteristics emerge from the figure. First, it is clear that both QuikSCAT and NCEP/NCAR data tend to underestimate the wind speed. Even though this can be expected from the NCEP/NCAR reanalyses, which represent the mean condition in a 2.5° × 2.5° box along 6 hours, it is not clear to us why QuikSCAT data present the same feature. On the other hand, there is a good general consistency in the wind direction between the different series. Other periods, when the number of atmospheric data collected in Pontón Recalada allowed for the comparison, were explored with similar results. Therefore, if wind data are to be used only qualitatively, NCEP/NCAR seems to be a good source.

[33] The pseudo wind stress vectors (defined as $\mathbf{W} \cdot |\mathbf{W}|$, where $\mathbf{W}$ is the wind vector) derived from the NCEP/NCAR reanalyses winds were therefore drawn together with the wavelet transform results from ARG (Figure 8) and PON (Figure 12). In order to eliminate very high frequency variability, a five-element moving average filter was applied to wind data prior to the pseudo stress computation. Some interesting results come from the simultaneous analysis of

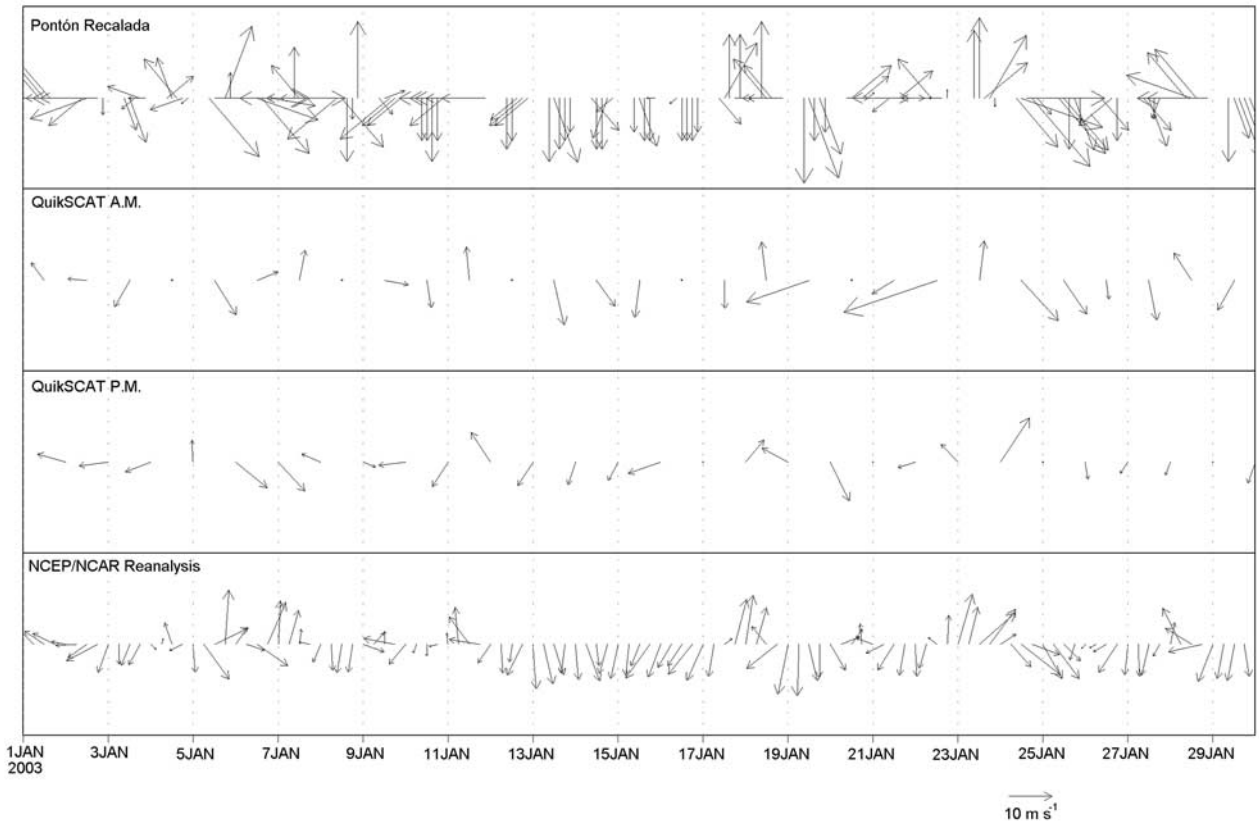

Figure 14. Wind vectors for January 2003 coming from portable rotating-cup anemometer observations collected in (top) Pontón Recalada, (middle) the nearest QuikSCAT scatterometer observation, and (bottom) the nearest point of the NCEP/NCAR reanalyses.

wind stress and scaleograms in ARG (Figure 8). First, there is a tendency for the internal waves to occur under conditions of calm or winds with a southward component (northwesterly to northeasterly winds). Reciprocally, in general, there is no wave activity in the cases when wind presents a southerly component. Both observations are qualitatively consistent with physical mechanisms for favorable or unfavorable conditions for internal wave generation, respectively. In this area, under northerly winds an extension of the surface fresh water plume to the east is expected; it would extend the salt wedge, giving as a result a more favorable environment for internal wave generation. Southerly winds are often intense, as they are associated with southeasterly and southwesterly intense winds storms [*Escobar et al.*, 2004]. In opposition, they would tend to produce intrusion of salty water and vertical mixing, destroying the density structure [*Guerrero et al.*, 1997] and hence inhibiting the internal wave development.

[34] Results indicate that in ARG internal wave activity was weaker and less frequent during the observed fall than throughout the sampled summer. Observations of the vertical density structure in the area indicate that the salt wedge is a semipermanent feature in this region; it is present unless persistent moderate to intense winds with a southerly component blow over the area producing vertical mixing [*Guerrero et al.*, 1997] and destroying the stratification. Nevertheless, these observations also show differences in the characteristics of this vertical density structure from one to another season. During fall a mean intensification of the vertical gradient with respect to summer and a similar horizontal extension of the salt wedge are expected [*Guerrero et al.*, 1997]. Therefore the mean conditions could be more favorable for internal waves during fall than in summer. Consequently, the larger number of events in summer cannot be explained in terms of the mean density structure. Nevertheless, it can be seen in Figure 8 that in ARG, southwesterly to southeasterly winds, which are likely to destroy the stratification, were considerably more frequent during April, and particularly May, 2003 than during the other sampled months. It suggests that the lack of internal wave activity during that fall could be, at least in part, the result from a period of nonfavorable conditions due to a high frequency of storms. Wind statistics suggest that this condition could be a typical one. The maximum frequency of intense southeasterly winds in the region occurs during summer and the beginning of fall and spring [*Fernandez and Necco*, 1975; *Escobar et al.*, 2004], whereas the maximum frequency of southwesterly winds occurs during the end of fall and beginning of winter [*Fernandez and Necco*, 1975; *Simionato et al.*, 2005]. If the frequency of winds from southeast to southwest is considered as a whole, summer is the less active season in terms of those winds, whereas maxima are observed during winter and beginning of spring.

[35] Wind stress vectors and amplitude scaleograms corresponding to PON are given in Figure 12, where it

can be seen that, similarly to ARG, most of the events in the diurnal band seem to occur under northerly winds and almost no internal wave activity can be observed under southerly winds. Nevertheless, for the observed period, events are less frequent than in ARG. As discussed in section 1, the thermohaline structure in PON differs from the one observed in ARG almost all along the year. PON observations were collected during spring and summer. During these seasons, the salt wedge structure is not a permanent condition in this part of the estuary [*Guerrero et al.*, 1997]. Its existence depends on the equilibrium between the continental runoff and the winds. In this area, and especially during summer, the continental discharge can play an important role in defining the mean position of the surface frontal zone. It is known that in years when runoff is very low, this front can move to approximately the longitude of Montevideo [*Mianzan et al.*, 2001]. Nevertheless, in short timescale, winds probably dominate the motions of the surface plume. *Simionato et al.* [2004b] modeled the estuary circulation under the different wind directions. Their results show that PON is located in a particular area, where the response to winds is not only related to their direction. There the convergence of conditions that produce a proper environment for internal wave generation is probably less frequent. This could explain, in turn, why the frequency of the events observed in PON is lower than the one observed in ARG.

[36] With regard to the forcing mechanisms, waves can be excited by a forcing in the appropriate frequency or can be free modes resulting from a relaxation. This last, for example, seems to be the case of the inertial wave detected during the first days of February 2003 in ARG (Figures 8 and 9), where a relaxation of the winds to calm conditions after almost 3 days of persistent northerly winds occurred. The semidiurnal oscillations registered in PON seem to be forced by the semidiurnal tide; the observed waves do not only have a period of around 12.5 hours, but also exhibit the zonal dominancy that characterizes the semidiurnal tidal constituents in the area (see Figure 4). About oscillations observed in the diurnal band, the fact that the waves seem to occur almost always under calm or northerly winds conditions is suggestive. This is especially the case in PON, where northerly winds could act, weakening the vertical density gradient. If this fact is considered together with other evidence arising from the results previously shown, the land/sea breeze emerges as a possible candidate. In PON, it has been shown that the internal wave signature in the diurnal band is stronger in the meridional than in the zonal velocity component. In this area the coast has a zonal orientation, and therefore land/sea breeze develops mainly in the meridional one [*Berri and Nuñez*, 1993; *Sraibman and Berri*, 2002]. In ARG, where the orientation of the coast is from northwest to southeast and breeze has zonal and meridional components of similar amplitude, wave signature observed in the diurnal band is intense for both velocity components. Land/sea breeze occurs mainly during warm and sunny days, especially during summer, and usually under mean winds with a northerly component [*Berri and Nuñez*, 1993; *Sraibman and Berri*, 2002]. In this sense, it is consistent that in PON, where data were collected during the warm season, internal wave activity is uniformly observed along the records, whereas in ARG, waves are present during the summer period of the records but decay during fall. Therefore the decay of internal wave activity during the autumn observed in ARG could also be explained in terms of lack of an appropriate forcing. During this season, both a larger number of storms. tending to destroy the stratification, and a lower number of days with land/sea breeze converge. The observed seasonality probably results from a combination of these two factors. If this is the case, winter can be expected to be a period of very weak to null internal wave activity, given that those adverse conditions are even more marked during that season.

4. Conclusions

[37] In this paper the first long period, high vertical and temporal resolution velocity time series collected in the Río de la Plata estuary salinity front were explored for periods less than 30 hours. Data were collected at two locations, one on the southern portion of the estuary in front of Samborombón Bay and the other on the northern portion, close to Montevideo. Data of the first series correspond to summer and autumn seasons whereas the second corresponds to spring and summer. Series were analyzed for their barotropic and baroclinic components. Barotropic component shows characteristics for both the tidal and mean currents, which is consistent with what is known about the circulation in the estuary. The dominant tidal constituent is M_2 in both locations. Consistent with numerical simulations, in the southern station, M_2 tidal ellipse has a clockwise rotation and a west-northwest to east-southeast orientation. Similar characteristics are displayed by the other semidiurnal constituents, such as N_2 and S_2. In the northernmost location the semidiurnal constituents are very elongated with an east-west orientation and M_2 has a counterclockwise rotation. In both locations the diurnal constituents O_1, K_1, and Q_1 significantly contribute to tidal currents in that order of importance. In all the records, tidal currents at the M_4 frequency are comparable to the ones related to Q_1 and S_2, indicating that nonlinear interaction is an important feature of the area. The mean barotropic currents show, in both locations, a different speed and direction, being in every case consistent with the seasonal excursion of the fresh water plume shown by historical salinity data.

[38] The baroclinic component of the currents provides the first observational evidence of the occurrence of internal waves in the frontal zone of the Río de la Plata estuary. Our results indicate that these baroclinic oscillations can account for as much as half of the total velocity variance in periods less than 30 hours, with related speeds of around 0.5 m s^{-1}. Differences in the wave's periods are observed from the northernmost to the southernmost location of observation. In the first case, essentially zonal oscillations with semidiurnal period and oscillations with a dominant meridional component and diurnal period are observed. Whereas the first one could be related to the dominant semidiurnal tide in the area, the second one seems to be atmospherically forced by land/sea breeze. In the southernmost location, oscillations of similar amplitude in the zonal and meridional currents were observed with periods around the inertial

and diurnal ones. Some of the inertial oscillations detected could result from wind relaxation, whereas oscillations in the diurnal band seem to be, as in the other location, forced by the land/sea breeze.

[39] Internal wave activity in the diurnal band is less frequent in the northernmost location than in the southernmost one. This fact can be attributed to less frequent favorable stratification conditions for internal wave generation in that area, at least during summer.

[40] Observations indicate that internal wave activity in the southernmost location was weaker, for the observed year, during fall than throughout the summer. This could be a typical feature given that during autumn, both the number of storms mixing the water column and destroying the thermohaline structure increases and appropriate conditions for breeze are less frequent. The fact that these conditions are even more marked during winter suggests that internal wave activity in the 24-hour band probably presents a seasonal cycle in the area.

[41] Internal waves are important as they can have an effect on mixing and sediment resuspension and transport. Presumably, they can also affect the marine fauna, given that the salinity front is a region of spawning for several coastal species during the warm season.

[42] Unfortunately, only tentative conclusions could be drawn in this paper with regard to the generation mechanisms for these waves. For example, even though it seems obvious to relate the semidiurnal wave observed in the Uruguayan side to the semidiurnal tide, the reasons why internal waves in this period are not observed in the Argentinean side and the mechanisms through which waves are excited are unclear. Likewise, it is also uncertain why inertial oscillations are not found in the Uruguayan side, whereas they are clearly observed in the Argentinean one. In order to make a better analysis, further and more comprehensive observations, including the thermohaline structure and atmospheric variables, are necessary. Numerical models could be extremely useful tools to help in understanding the excitation mechanisms and propagation processes.

[43] Finally, the way in which tidal currents are measured in the region must be reviewed. Classically, tidal currents in the Río de la Plata have been observed using a single level instrument. If the area where current observations are collected is active in terms of internal waves, the thus obtained results can be completely misleading. Therefore, simultaneous measurements of the density structure and the use of multilevel current meters are recommended.

[44] **Acknowledgments.** This paper is a contribution to the UNDP/GEF RLA/99/G31 Project "Environmental Protection of the Río de la Plata and its Maritime Front," the PICT 2002 07-12246 "Estudio de la dinámica oceánica y atmosférica del estuario del Río de la Plata mediante un sistema de modelado numérico integral," and the UBA grant X264. Authors are grateful to Simon Courret for his collaboration in data processing and analysis of barotropic tidal currents.

References

Balay, M. A. (1961), El Río de la Plata entre la atmósfera y el mar, *Publ. H-621*, 153 pp., Serv. de Hidrogr. Nav. Armada Argentina, Buenos Aires.

Bava, J. (2004), Metodologías de procesamiento de imágenes NOAA-AVHRR y su utilización en aplicaciones oceanográficas y biológico-pesqueras en el Atlántico Sudoccidental, Ph.D. thesis, 214 pp., Dep. of Cienc. Biol.., Fac. de Cienc. Exactas y Nat., Univ. de Buenos Aires, Argentina.

Berri, G. J., and M. N. Nuñez (1993), Transformed shoreline-following horizontal coordinates in a mesoscale model: A sea-land-breeze case study, *J. Appl. Meteorol.*, *32*(5), 918–928.

Boschi, E. E. (1988), El ecosistema estuarial del Río de la Plata (Argentina y Uruguay), in *Anales del Instituto de Ciencias del Mar y Limnología*, vol. 15, pp. 159–182, Univ. Nac. Autónoma de México, México City.

Campos, J. D., C. A. Lentini, J. L. Miller, and A. R. Piola (1999), Interannual variability of the sea surface temperature in the South Brazilian Bight, *Geophys. Res. Lett.*, *26*(14), 2061–2064.

Comisión Administradora del Río de la Plata (CARP) (1989), Estudio para la evaluación de la contaminación en el Río de la Plata, report, 137 pp., Inf. Comisión admin. del Río de la Plata, Buenos Aires.

Cousseau, M. B. (1985), Los peces del Río de la Plata y su Frente Marítimo, in *Fish Community Ecology in Estuaries and Coastal Lagoons: Towards an Ecosystem Integration*, edited by A. Yañez-Arancibia, pp. 515–534, UNAM Press Mexico, Mexico City.

D'Onofrio, E., M. Fiore, and S. Romero (1999), Return periods of extreme water levels estimated for some vulnerable areas of Buenos Aires, *Cont. Shelf Res.*, *19*, 1681–1693.

Dragani, W. C., C. G. Simionato, and M. N. Nuñez (2002), On the vertical structure of currents in the intermediate Río de la Plata: Observational study, *Geoacta*, *27*, 71–84.

Escobar, G., W. Vargas, and S. Bischoff (2004), Winds tides in the Río de la Plata estuary: Meteorological conditions, *Int. J. Climatol.*, *24*, 1159–1169.

Fernandez, A., and G. Necco (1975), Distribuciones de frecuencias de viento troposférico en estaciones argentinas período: 1958–1971: Tomo 1, internal report, 356 pp., Dep. de Cienc. de la Atmós. y los Océanos de la Fac. de Cienc. Exactas y Nat., Univ. de Buenos Aires, Buenos Aires, Argentina.

Foreman, M. G. G. (1978), Manual for tidal currents analysis and prediction, *Pac. Mar. Sci. Rep. 78-6*, 65 pp., Inst. for Ocean Sci., Patricia Bay, Sidney, B.C., Canada.

Framiñan, M. B., and O. B. Brown (1996), Study of the Río de la Plata turbidity front: I. Spatial and temporal distribution, *Cont. Shelf Res.*, *16*, 1259–1282.

Framiñan, M. B., M. P. Etala, E. M. Acha, R. A. Guerrero, C. A. Lasta, and O. B. Brown (1999), Physical characteristics and processes of the Río de la Plata Estuary, in *Estuaries of South America: Their Morphology and Dynamics*, edited by G. M. E. Perillo, M. C. Piccolo, and M. Pino Quivira, pp. 161–194, Springer, New York.

Gill, A. (1982), *Atmosphere-Ocean Dynamics*, *Int. Geophys. Ser.*, vol. 30, 662 pp., Elsevier, New York.

Glorioso, P. D., and R. A. Flather (1995), A barotropic model of the currents off SE South America, *J. Geophys. Res.*, *100*, 13,427–13,440.

Glorioso, P. D., and R. A. Flather (1997), The Patagonian Shelf tides, *Prog. Oceanogr.*, *40*, 263–283.

Guerrero, R. A., E. M. Acha, M. B. Framiñan, and C. A. Lasta (1997), Physical oceanography of the Río de la Plata Estuary, Argentina, *Cont. Shelf. Res.*, *17*, 727–742.

Jaime, P., A. Menéndez, M. Uriburu Quirno, and J. Torchio (2002), Análisis del régimen hidrológico de los ríos Paraná y Uruguay, *Inf. LHA 05-216-02*, 140 pp., Inst. Nac. del Agua, Buenos Aires, Argentina.

Kalnay, E., et al. (1996), The NCEP/NCAR 40-Year reanalysis project, *Bull. Am. Meteorol. Soc.*, *77*, 437–471.

Mianzan, H. W., E. Acha, R. Guerrero, F. Ramírez, D. Sorroarín, C. Simionato, and R. Borus (2001), South Brazilian marine fauna in the Río de la Plata estuary: Discussing the barrier hypothesis, paper presented at Colacmar IX, Asociación Latinoamericana de Invest. En Cienc. Del Mar, San Andrés, Isla, Colombia.

Naderi, F. M., M. H. Freilich, and D. G. Long (1991), Spaceborne radar measurement of wind velocity over the ocean—An overview of the NSCAT Scatterometer, *Proc. IEEE*, *79*, 850–866.

Piola, A. R., E. J. Campos, O. O. Möller, M. Charo, and C. Martinez (2000), Subtropical Shelf Front off eastern South America, *J. Geophys. Res.*, *105*, 6565–6578.

Sepúlveda, H. H., A. Valle-Levinson, and M. Framiñan (2004), Observations of subtidal and tidal flows in the Río de la Plata Estuary, *Cont. Shelf Res.*, *24*, 509–525.

Simionato, C. G., M. N. Nuñez, and M. Engel (2001), The Salinity Front of the Río de la Plata: A numerical case study for winter and summer conditions, *Geophys. Res. Lett.*, *28*(13), 2641–2644.

Simionato, C., W. Dragani, M. Nuñez, and M. Engel (2004a), A set of 3-D nested models for tidal propagation from the Argentinean Continental Shelf to the Río de la Plata Estuary: I. M2, *J. Coastal. Res.*, *20*(3), 893–912.

Simionato, C. G., W. Dragani, V. Meccia, and M. Nuñez (2004b), A numerical study of the barotropic circulation of the Río de La Plata Estuary: Sensitivity to bathymetry, Earth rotation and low frequency wind variability, *Estuarine Coastal Shelf Sci.*, *61*, 261–273.

Simionato, C., C. Vera, and F. Siegismund (2005), Surface wind variability on seasonal and interannual scales over Río de la Plata area, *J. Coastal Res.*, in press.

Sraibman, L., and G. J. Berri (2002), Experimentos con un modelo en ecuaciones primitivas de circulación atmosférica en capas bajas sobre el Río de la Plata y su zona de influencia, paper presented at XXI Reunión Científica AAGG 2002, Asociación Argentina de Geofís. y geodestas, Rosario, Argentina.

Torrence, C., and G. Compo (1998), A practical guide to wavelet analysis, *Bull. Am. Meteorol. Soc.*, *79*, 61–78.

Wu, C., J. Graf, M. Freilich, D. Long, M. Spencer, W. Tsai, D. Lisman, and C. Winn (1994), The Sea Winds scatterometer instrument, in *International Geoscience and Remote Sensing Symposium*, volume 3, edited by T. I. Stein, pp. 1511–1515, Inst. of Electr. and Electrón. Eng., Pisacataway, N. J.

W. Dragani, Departamento de Ciencias de la Atmósfera y los Océanos, FCEN, Universidad de Buenos Aires, Buenos Aires, Argentina.

V. Meccia, M. Nuñez, and C. G. Simionato, Centro de Investigaciones del Mar y la Atmósfera (CIMA/CONICET-UBA), Ciudad Universitaria Pabellón II Piso 2(C1428EHA), Buenos Aires 1428, Argentina. (claudias@cima.fcen.uba.ar)